

# Subgrid-Scale Contribution to Noise Production in Decaying Isotropic Turbulence

Christelle Seror\* and Pierre Sagaut†  
ONERA, 92322 Châtillon Cedex, France

and

Christophe Bailly‡ and Daniel Juvé§  
École Centrale de Lyon, 69131 Ecully Cedex, France

An estimation of the noise generated by subgrid scales provided by a large-eddy simulation (LES) calculation is performed based on a priori tests. The derivation of Navier–Stokes equation to obtain Lighthill’s equation (Lighthill, M. J., “On Sound Generated Aerodynamically, Part I: General Theory,” *Proceedings of the Royal Society of London*, Vol. A211, 1952, pp. 564–587; Lighthill, M. J., “On Sound Generated Aerodynamically, Part II: Turbulence as a Source of Sound,” *Proceedings of the Royal Society of London*, Vol. A222, 1954, pp. 1–32) is presented for both the direct numerical simulation (DNS) and the LES Navier–Stokes equations. The Lighthill tensor is split into several parts: a high-frequency part that is not resolved by LES calculation, the filtered Lighthill tensor computed from basic filtered variables, and a subgrid-scale tensor. A DNS of decaying isotropic turbulence is carried out to evaluate the contribution of each term to the noise production. It is confirmed that the high-frequency part of Lighthill’s tensor does not contribute significantly to noise production for the usual cutoff wave number value of LES. The subgrid-scale contribution cannot be neglected and requires the use of a subgrid-scale model to recover reliable results dealing with the acoustic field. The acoustic contribution computed using a subgrid-scale model of scale similarity type is compared to the acoustic contribution of the exact subgrid-scale tensor.

## Nomenclature

$c_0$	= speed of sound
$D$	= computational length
$G$	= filter function
$K$	= turbulent kinetic energy
$k_c$	= normalized cutoff wave number
$L$	= initial integral length scale
$M$	= Mach number
$M_t$	= turbulent Mach number
$Pr$	= Prandtl number
$Re$	= Reynolds number
$Re_\lambda$	= Taylor microscale Reynolds number
$u^{\text{rms}}$	= rms velocity
$V$	= computational domain
$\mathbf{x}$	= observer position
$\mathbf{y}$	= local source position
$\gamma$	= specific heat ratio
$\delta_{ij}$	= Kronecker tensor
$\epsilon$	= turbulent dissipation rate
$\lambda$	= Taylor microscale
$\mu$	= dynamic viscosity
$\nu$	= molecular kinetic viscosity
$\tau$	= initial eddy turn over time

## Subscript

0 = computed; time  $t$  equals 0

## Superscripts

LES = large-eddy simulation quantity computed from the filtered variables

SGS = subgrid scale quantity  
" = high-frequency quantity

## I. Introduction

SOUND generated by turbulence raises many questions of fundamental and engineering interest. Initial work especially was based on analytical and experimental results, but recent progress in computational fluid dynamic (CFD) offers many tools to develop new techniques in computational aeroacoustics (CAA). Because the acoustic source originates in turbulent fluctuations, the resolution of the acoustic field is difficult as a result of the wide range of spatial and temporal frequencies.<sup>1</sup> Complete knowledge of the unsteady aerodynamic field cannot be reached in practical configurations of interest. A steady statistical description of the turbulent flow has long been used<sup>2,3</sup> before numerical simulations were carried out to compute the aerodynamic field.<sup>4</sup>

Direct numerical simulation (DNS),<sup>5</sup> unsteady Reynolds averaged Navier–Stokes simulations,<sup>6</sup> semideterministic modeling,<sup>7,8</sup> or, as detailed in this paper, large eddy simulation (LES),<sup>9,10</sup> are used to compute the acoustic source, that is, the unsteady flowfield. The DNS approach does not allow the computation of high-Reynolds-number turbulent flows that have to be dealt with in practice. Because noise radiated from turbulent flow is generated especially from large-scale motion,<sup>9</sup> LES, which is based on the resolution of low wave number components (referred to as  $\bar{u}$ ) and on the parameterization of high wave number components (referred to as  $u''$ ) of turbulent quantities, is very attractive to resolve such problems. CAA then offers many possibilities to calculate the sound field radiated by turbulent fluctuations: Lighthill’s analogy<sup>11,12</sup> retained for the present work, a third-order wave equation, namely, Lilley’s equation,<sup>13</sup> or the linearized Euler’s equations. Each of these possibilities requires knowledge of the aerodynamic field. Lighthill’s analogy, which is based on the solution of Lighthill’s equation derived from the compressible Navier–Stokes equations, was the first attempt to estimate the sound radiated from a finite region of turbulent flow. This method is a very powerful and general approach to compute the acoustic radiated field, although it has the limitation of assuming that the refraction effect cannot be taken into account. By the use of this analogy, the pressure generated by a turbulent flow is expressed as a function of the Lighthill<sup>11,12</sup> tensor  $T_{ij} \approx \rho u_i u_j$ .

Received 27 January 1999; revision received 1 March 2000; accepted for publication 18 March 2000. Copyright © 2000 by the authors. Published by the American Institute of Aeronautics and Astronautics, Inc., with permission.

\*Ph.D. Student, DSNA, 29 av. de la Division Leclerc.

†Scientist Engineer, DSNA, 29 av. de la Division Leclerc.

‡Assistant Professor, Laboratoire de Mécanique des Fluides et d’Acoustique, 36 av. Guy de Collongue, BP 163. Member AIAA.

§Professor, Laboratoire de Mécanique des Fluides et d’Acoustique, 36 av. Guy de Collongue, BP 163. Member AIAA.

In LES calculations, only the filtered variables  $\tilde{u}_i$  are available, and so the Lighthill tensor cannot be computed in its complete form. A Lighthill tensor  $T_{ij}^{\text{LES}} = \tilde{\rho} \tilde{u}_i \tilde{u}_j$  calculated with the basic filtered variables is often used.<sup>9,10</sup> The aerodynamic field does not contain all frequencies available, but only the low-frequency part of the field. The importance of this may be relevant for aeroacoustic computations and must be estimated.

Piomelli et al.<sup>14</sup> proposed a correction based on LES properties to recover interactions between the large and subgrid scales. The Lighthill<sup>11,12</sup> tensor was corrected by adding a subgrid-scale tensor. On the ground of a wind channel simulation, the effect of filtering and the subgrid scale tensor parameterization were proposed for the acoustic source term.

This paper addresses the new problem of the evaluation and modeling the contribution of the unresolved scales to the radiated noise production, when Lighthill's<sup>11,12</sup> analogy is employed together with LES (namely, hybrid LES). Results are compared to those obtained when DNS is used together with Lighthill's analogy (hybrid DNS). The governing equations for hybrid DNS are first presented and extended to the case of hybrid LES approach in Sec. II. Section III is devoted to the evaluation of the subgrid and high-frequency contributions to the complete Lighthill tensor, based on a priori tests performed in the decaying isotropic turbulence case. Section IV deals with the parameterization of the subgrid-scale noise production, and results of a priori tests are discussed. Conclusions are presented in Sec. V.

## II. Mathematical Formulation

### A. Governing Equations for Hybrid DNS

For an ideal gas, the equations of motion, continuity, momentum, and energy conservation, can be recast in the following form:

$$\frac{\partial}{\partial t} \rho + \frac{\partial}{\partial y_j} \rho u_j = 0 \quad (1)$$

$$\frac{\partial}{\partial t} \rho u_i + \frac{\partial}{\partial y_j} \rho u_i u_j = \frac{\partial}{\partial y_j} (-p \delta_{ij} + \sigma_{ij}) \quad (2)$$

$$\frac{\partial}{\partial t} E + \frac{\partial}{\partial y_i} ((E + p) u_i) = \frac{\partial}{\partial y_j} (\sigma_{ij} u_i) - \frac{\partial}{\partial y_i} Q_i \quad (3)$$

where  $\rho$ ,  $u_i$ ,  $p$ , and  $E$  are the density, the velocity components, the thermodynamic pressure and the total energy, respectively.

The viscous stress tensor  $\sigma_{ij}$  is defined as

$$\sigma_{ij} = -\frac{2}{3} \frac{\mu}{Re} \frac{\partial}{\partial y_k} u_k \delta_{ij} + \frac{\mu}{Re} \left( \frac{\partial}{\partial y_i} u_j + \frac{\partial}{\partial y_j} u_i \right) \quad (4)$$

The heat flux vector  $Q_i$  is written as follows:

$$Q_i = -\frac{\mu}{(\gamma - 1) Re Pr M^2} \frac{\partial}{\partial y_i} \Theta \quad (5)$$

where  $\Theta$  is the temperature. For an airflow, the specific heat ratio is  $\gamma = 1.4$  and the Prandtl number  $Pr = 0.7$ .

These equations must be supplemented with the equation of state:

$$p = (1/\gamma M^2) \rho \Theta \quad (6)$$

One of the first attempts to estimate the sound radiated from a finite region of turbulent flow was proposed by Lighthill.<sup>11,12</sup> The combination  $\partial/\partial t$  [Eq. (1)] –  $\partial/\partial y_i$  [Eq. (2)] leads to Lighthill's wave equation for the density:

$$\frac{\partial^2}{\partial t^2} \rho - c_0^2 \frac{\partial^2}{\partial y_i \partial y_i} \rho = \frac{\partial^2}{\partial y_i \partial y_j} T_{ij} \quad (7)$$

where  $c_0$  is the constant speed of sound in the ambient medium and the Lighthill tensor  $T_{ij}$  is defined as follows:

$$T_{ij} = \rho u_i u_j + (p - c_0^2 \rho) \delta_{ij} - \sigma_{ij} \quad (8)$$

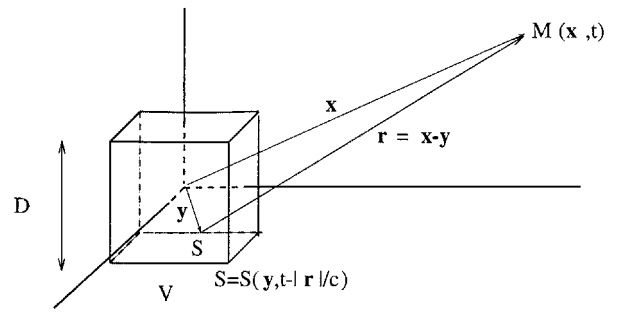


Fig. 1 Geometry of sound source radiation:  $V$  = volume of turbulent fluid,  $M$  = observer position, and  $D = 2\pi$ .

For high Reynolds number, the viscous stress tensor  $\sigma_{ij}$  in Lighthill's tensor expression can be neglected. For low turbulent Mach number, the pressure perturbations are assumed to be nearly isentropic, and the acoustic pressure can then be written as  $p = c_0^2 \rho$ . Under these assumptions, Lighthill's tensor simplifies to

$$T_{ij} = \rho u_i u_j \quad (9)$$

The solution of Eq. (7) is exact only for a homogeneous medium at rest. To obtain an integral formulation, Green's function is required. Thus, the fluctuating density<sup>9,15</sup> can be expressed as a function of the Lighthill tensor:

$$\rho'(x, t) = \frac{1}{4\pi c_0^4} \frac{x_i x_j}{x^3} \int_V \left[ \frac{\partial^2}{\partial t^2} T_{ij} \right] - \left\langle \left[ \frac{\partial^2}{\partial t^2} T_{ij} \right] \right\rangle d^3 y \quad (10)$$

where the brackets denote the evaluation at the retarded time  $t - r/c_0$ , where  $r = |\mathbf{x} - \mathbf{y}|$  is the vector joining the source point  $\mathbf{y}$  to the observation point  $\mathbf{x}$ , as shown in Fig. 1, and  $\langle \rangle$  denotes statistical average.

As soon as the aerodynamic field is known, the fluctuating acoustic density can be computed. For high Reynolds numbers, a DNS cannot be carried out because of the very high computational cost, and then statistical models are used to account for a part of the turbulent fluctuations. LES offers the possibility to compute high-Reynolds-number turbulent flows by resolving large eddies and parameterizing small eddies. The description of the governing equation when LES and Lighthill's<sup>11,12</sup> analogy are used together is presented in the following section.

### B. Extension to LES

In LES of compressible turbulent flows, any quantity  $F$  in the flow domain  $V$  can be decomposed into a resolved or filtered part  $\bar{F}$  and an unresolved or subgrid part  $f$  through the application of a low-pass convolution filter:

$$F = \bar{F} + f \quad (11)$$

with

$$\bar{F}(\mathbf{y}) = \int_V G_\Delta(\mathbf{y} - \boldsymbol{\xi}) F(\boldsymbol{\xi}) d\boldsymbol{\xi} \quad (12)$$

where  $G_\Delta$  is the filter kernel and  $\Delta = \pi/k_c$  the characteristic cutoff length scale. The filter kernel  $G_\Delta$  is a spatial filter (usually a sharp cutoff filter in Fourier space or a Gaussian filter) of width usually assumed to be equal to the grid spacing. When dealing with variable density flows, the mass-weighted variables  $\tilde{F}$  are used, following Favre,<sup>16</sup> with

$$\tilde{F} = \overline{\rho F} / \bar{\rho} \quad (13)$$

Thus, the quantity  $F$  is now decomposed as

$$F = \tilde{F} + F'' \quad (14)$$

By the use of this definition, the Favre filtered continuity and momentum equations are

$$\frac{\partial}{\partial t} \bar{\rho} + \frac{\partial}{\partial x_j} \bar{\rho} \tilde{u}_j = 0 \quad (15)$$

$$\frac{\partial}{\partial t} \bar{\rho} \tilde{u}_i + \frac{\partial}{\partial y_j} \bar{\rho} \tilde{u}_i \tilde{u}_j + \frac{\partial}{\partial y_i} \bar{p} = \frac{\partial}{\partial y_j} \tilde{\sigma}_{ij} - \frac{\partial}{\partial y_j} \tau_{ij} \quad (16)$$

The term  $\tau_{ij}$  is a subgrid quantity resulting from the nonlinearity of the convective terms and is defined as

$$\tau_{ij} = \bar{\rho} (\widetilde{u_i u_j} - \tilde{u}_i \tilde{u}_j) \quad (17)$$

Following the Vreman et al. approach<sup>17</sup> and according to Brandsma's assumptions,<sup>18</sup> the Favre<sup>16</sup> filtered energy equation is straightforward.

The filtered Lighthill equation can be obtained in two ways: by operating the combination of the filtered continuity equation and filtered momentum equation, that is,  $\partial/\partial t$  [Eq. (15)] –  $\partial/\partial y_i$  [Eq. (16)], or by filtering the Lighthill Eq. (7). In both cases, the resulting equation for resolved (or filtered) density is

$$\frac{\partial^2}{\partial t^2} \bar{\rho} - c_0^2 \frac{\partial^2}{\partial y_i \partial y_i} \bar{\rho} = \frac{\partial^2}{\partial y_i \partial y_j} \widetilde{T}_{ij} \quad (18)$$

where the filtered Lighthill tensor  $\widetilde{T}_{ij}$ , which represents the production of resolved acoustic fluctuations, is then given by

$$\widetilde{T}_{ij} = \bar{\rho} \widetilde{u_i u_j} \quad (19)$$

The filtered Lighthill tensor differs from  $T_{ij}$  by  $T_{ij}''$ , the high-frequency part of the complete Lighthill tensor that is not resolved in LES calculations. The resulting decomposition of  $T_{ij}$  is given by

$$T_{ij} = \widetilde{T}_{ij} + T_{ij}'' \quad (20)$$

Because the basic variables of LES calculations are  $\bar{\rho}$  and  $\tilde{u}_i$ , the source term  $\widetilde{T}_{ij}$  cannot be directly computed and must be approximated by  $T_{ij}^{\text{LES}} = \bar{\rho} \tilde{u}_i \tilde{u}_j$  with an inherent error  $T_{ij}^{\text{SGS}}$ , which is actually the subgrid scale (SGS) tensor  $\tau_{ij}$  defined in Eq. (17):

$$\widetilde{T}_{ij} = T_{ij}^{\text{LES}} + T_{ij}^{\text{SGS}} = \bar{\rho} \tilde{u}_i \tilde{u}_j + \tau_{ij} \quad (21)$$

The final decomposition for the full Lighthill tensor is then written as

$$T_{ij} = T_{ij}^{\text{LES}} + T_{ij}^{\text{SGS}} + T_{ij}'' \quad (22)$$

To get reliable far-field noise prediction using LES calculations, the SGS tensor appears naturally as a source term in the expression of the acoustic fluctuating pressure and must be evaluated to assess the accuracy of a prediction of the far-field noise from LES simulations.

### III. A Priori Evaluation of the Subgrid Acoustic Source

#### A. Numerical Simulation Description and Validation

A priori tests were carried out to estimate the subgrid contributions to radiated noise from freely decaying isotropic turbulence. This case corresponds to a self-similar statistically nonstationary solution, but does not require the use of a random forcing term whose acoustic properties are unknown, as the forced isotropic turbulence case does.

DNS were performed on a  $N^3 = 72^3$  uniform spatial grid using a fourth-order-centered scheme for the convective terms, a second-order-centered scheme for the viscous terms, and a third-order Runge–Kutta scheme for the integration in time. The initial parameters of the simulation are  $N = 72$ ,  $Re_\lambda = 19$ ,  $M_t = 0.3$ ,  $L_0 = 0.64$ ,  $\lambda_0 = 0.5$ , and  $\eta_0 = 0.03$ .

In the simulation the Taylor microscale Reynolds number  $Re_\lambda = \lambda_0 K_0 / \nu$  is equal to 19, and the turbulent Mach number  $M_t = u_0^{\text{rms}} / c_0$  is equal to 0.3. The initial velocity field is chosen to

be solenoidal. This initial condition and the low value of the Mach number ensure that the flow will follow a quasi-incompressible behavior,<sup>19</sup> which allows the use of the reduced form of the Lighthill tensor given by Eq. (9).

The initial energy spectrum is given by

$$E(k) = k^4 \exp(-2k^2/k_0^2) \quad \text{with} \quad k_0 = 4 \quad (23)$$

At the beginning of the simulation, the mesh size  $\Delta y$  is such that  $\Delta y / \eta_0 = 2.95$ , where  $\eta_0 = (\nu^3 / \epsilon_0)^{1/4}$  is the Kolmogorov length scale at the initial time, and is in good agreement with DNS resolution requirements. Because we are dealing with freely decaying turbulence, the ratio  $\Delta y / \eta$  will decrease as the Kolmogorov scale increases, ensuring that the resolution is accurate enough to capture all of the relevant turbulent fluctuations during the whole simulation. Turbulence statistics presented hereafter are obtained by performing a statistical average over the computational domain and are presented as a function of the dimensionless time  $t^* = t / \tau_0$ , where  $\tau_0 = L_0 / u_0^{\text{rms}}$  is the initial large-eddy turnover time. The time decay of the normalized turbulent kinetic energy  $K(t^*) / K_0$  is shown in Fig. 2 and is found to be in agreement with classical results on that configuration. The normalized turbulent dissipation rate  $\epsilon(t^*) / \epsilon_0$ , plotted in Fig. 3, increases during the initial transient due to the generation of small-scale fluctuations through the nonlinear kinetic

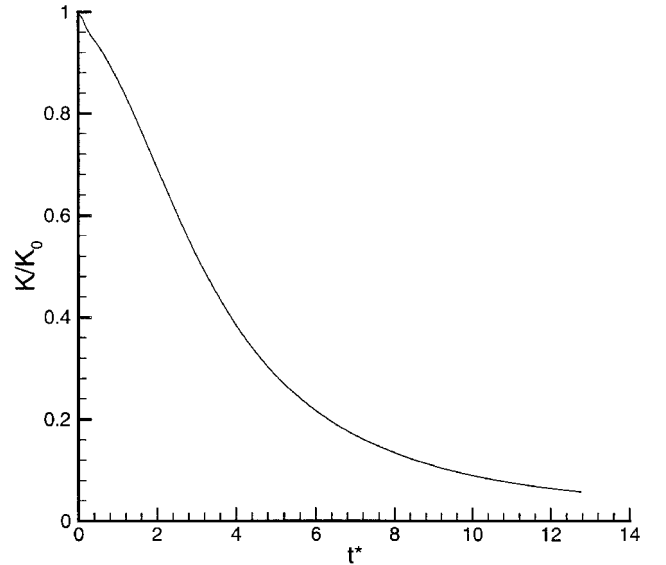


Fig. 2 Normalized kinetic energy  $K/K_0$  time history.

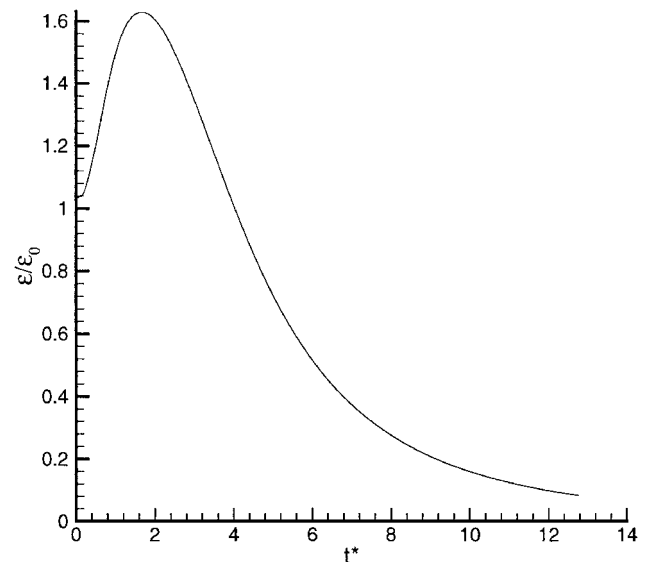


Fig. 3 Normalized dissipation  $\epsilon/\epsilon_0$  time history.

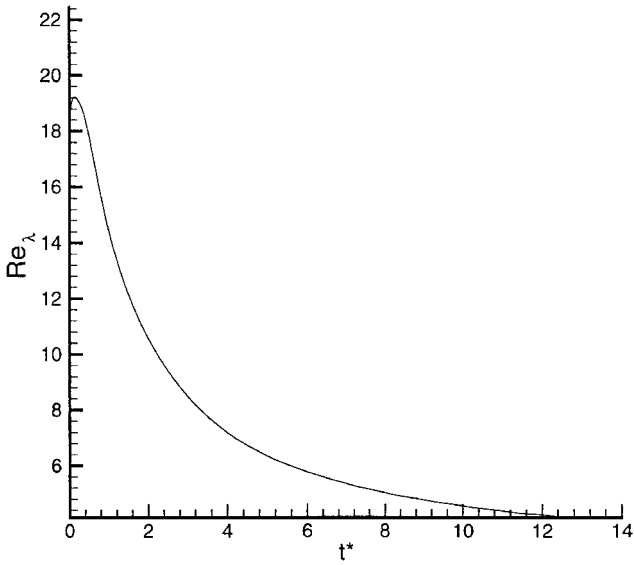


Fig. 4 Taylor microscale Reynolds number  $Re_\lambda$  time history.

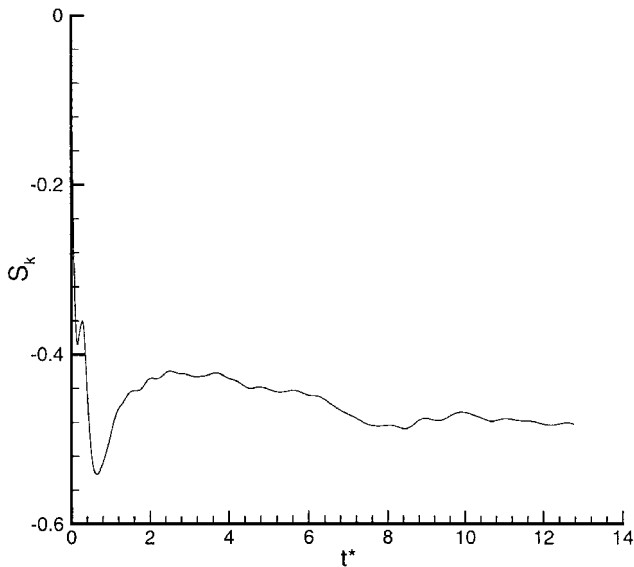


Fig. 5 Skewness  $S_k$  time history.

energy cascade process and finally decays in the absence of external forcing once the spectrum is full. The time evolution of the Taylor microscale Reynolds number  $Re_\lambda$  is shown in Fig. 4. The end of the acoustic calculations is chosen such that the Taylor microscale number has decreased by a factor of 3 from its initial value,  $Re_\lambda$  being too small at a later time to ensure a realistic representation of turbulence dynamics. The skewness factor of the velocity derivative  $S_k = \langle (\partial u / \partial x)^3 \rangle / \langle (\partial u / \partial x)^2 \rangle^{3/2}$  supplies a measure of the nonlinear vortex stretching. The experimental value for isotropic turbulence of  $S_k$  is  $-0.4$ , whereas our simulations give  $S_k \approx -0.5$  (Ref. 20). Results presented in Fig. 5 show that for the present calculations the skewness asymptotes to the value  $S_k \approx -0.48$ , leading to satisfactory agreement. As acoustic results are relevant when the decay of turbulence is self-similar,<sup>15</sup> the acoustic calculation is initialized at this time to avoid spurious nonequilibrium effects in the calculation of acoustic source terms. The normalized energy spectrum

$$E^* = \left[ E(k) / \int_0^\infty E(k) dk \right]$$

computed at time  $t^* = 3.55$  is plotted in Fig. 6. A  $k^{-5/3}$  slope is recovered on the interval  $5 \leq k \leq 10$ , in agreement with the Moin and Mahesh assertion<sup>21</sup> that a decade-wide inertial range is found

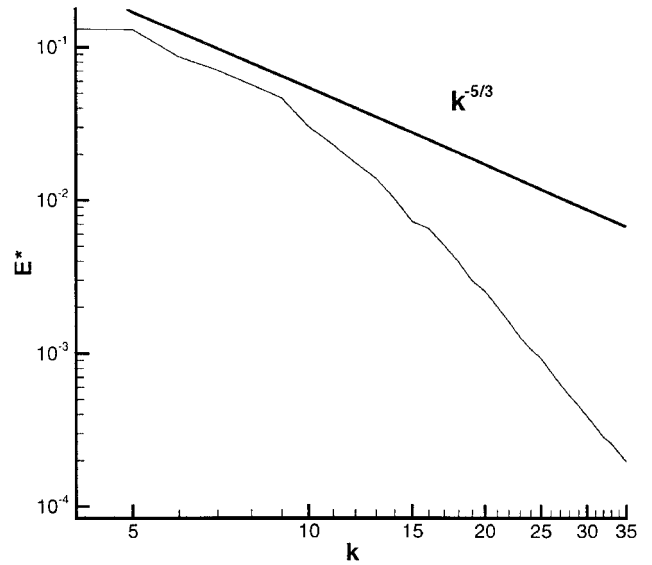


Fig. 6 Normalized energy spectrum at time  $t^* = 3.55$ .

only for  $Re_\lambda \geq 100$ . These results demonstrate the good quality of the simulation, which is suitable for a priori testing.

**B. Acoustic Quantities Computation**

The fluctuating pressure is computed<sup>9,15</sup> using Eq. (10):

$$p'(x, t) = \frac{1}{4\pi c_0^2} \frac{x_i x_j}{x^3} \int_V \left[ \frac{\partial^2}{\partial t^2} T_{ij} \right] - \left\langle \left[ \frac{\partial^2}{\partial t^2} T_{ij} \right] \right\rangle d^3 y \quad (24)$$

and the acoustic intensity is computed<sup>9</sup> as follows:

$$I = \frac{\langle [p'(x, t)]^2 \rangle}{\rho_0 c_0} \quad (25)$$

The ensemble average  $\langle \rangle$  is computed over six different, but statistically equivalent, simulations and for each simulation with 24 different observer points located at the same distance from the center of the computational domain  $V$ , yielding 144 samples. It was checked that this process ensures the convergence of statistical moments. The radiated acoustic pressure is computed at observer points distributed on six planes  $P_i$ ,  $i = 1, 6$ , parallel to the faces of the volume of turbulent fluid. Each plane  $P_i$  is located at the same distance,  $x = 10D = R_{\text{obs}}\pi$  from the center of the computational domain, where  $D$  is defined in Fig. 1, and each plane contains four observer points. One of the four observer points is located at the intersection between the line passing through the center of the cube and the plane  $P_i$ . The three others are distributed close to this one such that the time delay difference between these observer points is less than the time step and is neglected. The source points located on a sphere centered at the observer position contribute to the radiated noise at the same time. Because the acoustic far field is investigated, the sphere can be replaced by a plane such that only the time delay between planes perpendicular to the direction of  $x$  is taken into account to compute the retarded time in expression (10). An observer point  $O$  is considered and identified by the vector  $x_O = (\pi \times R_{\text{obs}}, 0, 0)'$  (where  $R_{\text{obs}} = 20$ ). The nearest source term is located on a sphere of radius  $(R_{\text{obs}} - 1)\pi$ . The assumption that this sphere can be replaced by a plane supposes that the time delay between the nearest source point  $A$  located at  $x_A = (\pi(R_{\text{obs}} - 1), 0, 0)'$  and one of the farther points on this plane located at  $x_B = [\pi(R_{\text{obs}} - 1), \pi, \pi]'$  is negligible. This time delay can be computed using  $\delta t = (d(O, B) - d(O, A))M$ , where  $d(O, A)$  is the distance between the observer position  $O$  and the point  $A$  and  $d(O, B)$  the distance between  $O$  and  $B$ :

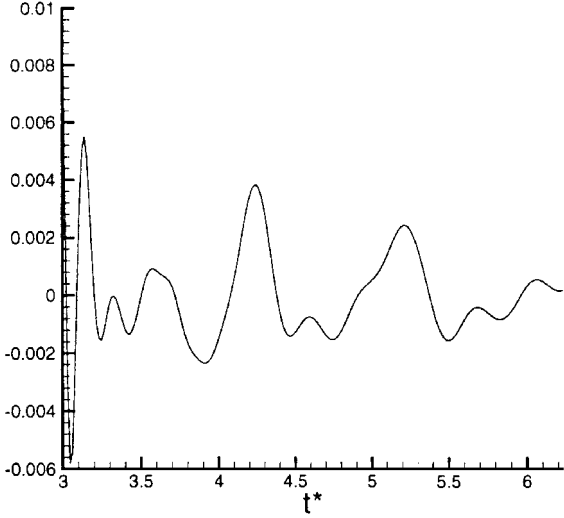
$$d(O, A) = (R_{\text{obs}} - 1)\pi$$

$$d(O, B) = (R_{\text{obs}} - 1)\pi \times \sqrt{1 + 1/2(R_{\text{obs}} - 1)^2}$$

$$\approx (R_{\text{obs}} - 1)\pi \times \left( 1 + 1/4(R_{\text{obs}} - 1)^2 \right)$$

**Table 1** Values and characteristics of  $k_c$  and  $\Delta$ 

$k_c$	4	6	8	10	12	14	16	18	20	22
$\Delta/\eta_0$	26.17	17.45	13.10	10.47	8.73	7.48	6.54	5.82	5.24	4.76
$\Delta/\lambda_0$	1.57	1.05	0.80	0.63	0.52	0.45	0.39	0.35	0.31	0.29
$\Delta/L_0$	1.23	0.89	0.61	0.49	0.41	0.35	0.30	0.27	0.25	0.22

**Fig. 7** Fluctuating acoustic pressure calculated from DNS data.

Thus, the time delay is

$$\delta t = (R_{\text{obs}} - 1)\pi \times (1/4(R_{\text{obs}} - 1)^2) \times M \approx 0.012$$

However, the characteristic time step for the aeroacoustics is given by  $\delta\tau = \Delta x \cdot M \approx 0.027 \geq \delta t$ . This affirms the assumption that the sphere can be replaced by a plane.

### C. Acoustical Results

The acoustic fluctuating pressure computed from DNS data using Eq. (24) is displayed in Fig. 7 as a function of time at an observer position. The pressure signal observes a general decay process induced by the decrease of the acoustic source term  $(\partial^2/\partial t^2)T_{ij}$  associated with the kinetic energy decay.

To access the exact acoustic pressure resulting from the SGS and the high-frequency part of the source term, Lighthill's tensors  $\tilde{T}_{ij}$  and  $T_{ij}^{\text{LES}}$  have been computed from DNS data according to Eq. (12). Two filters have been considered, namely, a Gaussian filter and a sharp spectral cutoff filter, whose associated kernel in physical space  $G_\Delta$  and transfer function  $\hat{G}$  are, respectively,

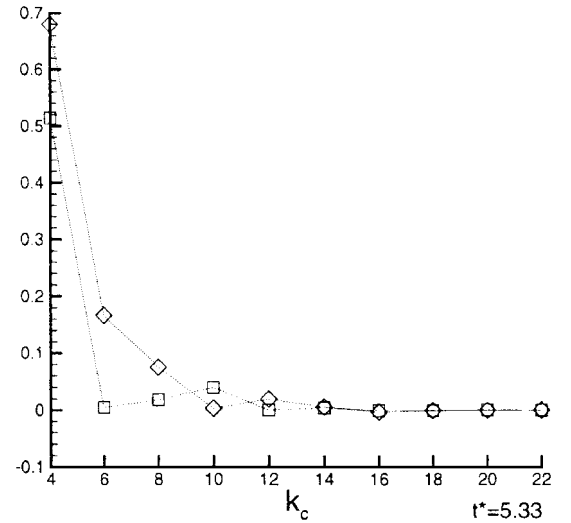
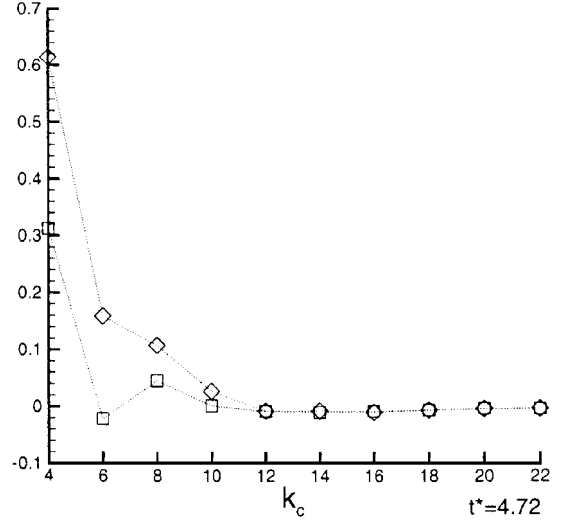
$$G_\Delta(\mathbf{y} - \boldsymbol{\xi}) = \left(\frac{6}{\pi\Delta^2}\right)^{\frac{3}{2}} \exp\left(\frac{-6|\mathbf{y} - \boldsymbol{\xi}|^2}{\Delta^2}\right)$$

$$\hat{G}(k) = \exp\left(\frac{-\Delta^2 k^2}{24}\right) \quad (26)$$

$$G_\Delta(\mathbf{y} - \boldsymbol{\xi}) = \frac{\sin[k_c(\mathbf{y} - \boldsymbol{\xi})]}{k_c(\mathbf{y} - \boldsymbol{\xi})}$$

$$\hat{G}(k) = \begin{cases} 1 & \text{if } |k| \leq k_c = \pi/\Delta \\ 0 & \text{else} \end{cases} \quad (27)$$

The Gaussian filter (26) induces a smooth separation between resolved and subgrid quantities, resulting in a nonzero contribution of low frequencies to the latter. On the contrary, the sharp spectral cutoff filter [Eq. (27)] prevents any contribution of low frequencies to SGS terms. The effect of the two filters has been investigated as a function of the normalized cutoff wave number  $k_c$ . Results are presented for values of the cutoff wave number  $k_c$  in Table 1. The

**Fig. 8** Evolution of the intensity of the unresolved noise by LES calculation  $I''/I$  as a function of the cutoff wave number  $k_c$  for two different times:  $\square$ , sharp cutoff filter, and  $\diamond$ , Gaussian filter.

ratio between the characteristic cutoff length scale and characteristic flow length scales  $\eta_0$ ,  $\lambda_0$ , and  $L_0$  respectively are reported in Table 1.  $\Delta/\eta_0$  indicates the resolution of the mesh in terms of the Kolmogorov length scale. LES models ensure reliable results for the aerodynamic field when the mesh size used in LES computations is such as  $\Delta \approx \lambda$ . This condition ensures most of the molecular diffusion effects are directly taken into account. Because the integral length scale is the characteristic large scale of the turbulent flow,  $\Delta$  is required to be less than  $L_0$  to ensure good resolution of the large eddies. Table 1 indicates that cutoff wave number values  $k_c \geq 8$  can then be used to compute the flowfield.

The difference between acoustic values computed from DNS data with the exact tensor  $T_{ij}$  and acoustic values obtained from the filtered tensor  $\tilde{T}_{ij}$  are investigated. This preliminary study allows the analysis of the acoustic properties of the high-frequency part of the acoustic source  $T_{ij}''$ . To emphasize the importance of the high-frequency part of the acoustic source, the intensity ratio  $I''/I = (I - \tilde{I})/I$  is computed as a function of  $k_c$  (Fig. 8), where  $\tilde{I}$  and  $I$  are the acoustic intensities, respectively, associated to the

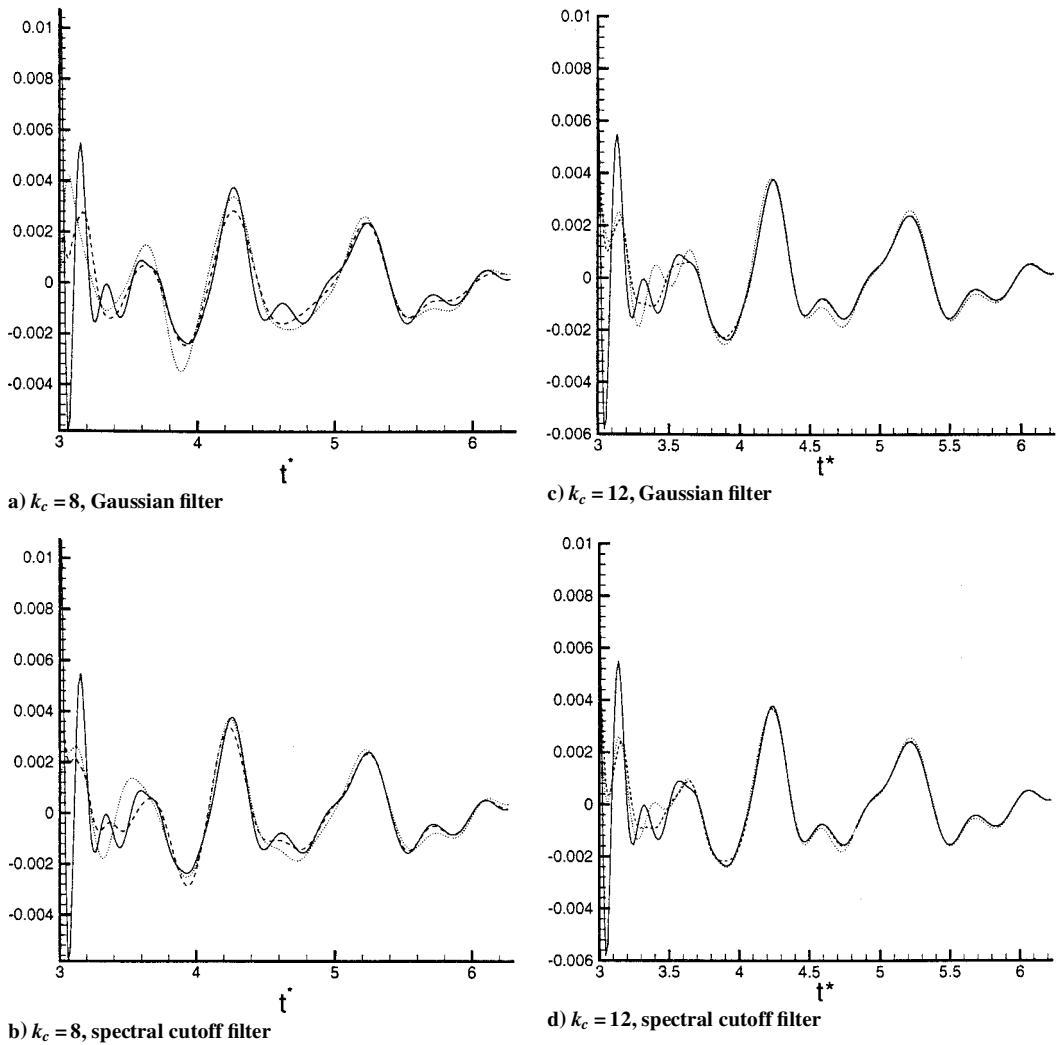


**Fig. 9** Comparison between the fluctuating acoustic pressures, —  $p'$ , ---  $\tilde{p}'$ , and ···  $p'^{\text{LES}}$ , respectively, computed from the exact Lighthill's tensor  $T_{ij}$  and from filtered Lighthill's tensors  $\tilde{T}_{ij}$  and  $T_{ij}^{\text{LES}}$ .

filtered source term  $\tilde{T}_{ij}$  and the full Lighthill tensor  $T_{ij}$ . Two different times are considered: the first,  $t^* = 4.74$ , corresponds to a maximal contribution of the SGS and the second,  $t^* = 5.33$ , to a small contribution of these modes. For both times, the intensity ratio tends rapidly to zero, and the intensity of the unresolved noise is less than 10% of the total intensity for  $k_c > 8$ . Because the unresolved noise is found to be small for both filters with cutoff wave number  $k_c > 8$ , it is deduced that exact LES calculations using  $\tilde{T}_{ij}$  can be suitable to compute the acoustic source and that the acoustic features of the considered turbulent flow are connected to the low-frequency part of the source. These results are in agreement with those obtained by Witkowska et al.<sup>9</sup> for the noise generation process in isotropic turbulence.

Additional a priori tests were carried out to estimate the low-frequency noise generated by the SGS stress tensor  $T_{ij}^{\text{SGS}}$ . To compare fluctuating acoustic pressures  $p'$ ,  $\tilde{p}'$ , and  $p'^{\text{LES}}$  associated to source terms  $T_{ij}$ ,  $\tilde{T}_{ij}$  and  $T_{ij}^{\text{LES}}$ , respectively, the spectral cutoff filter and the Gaussian filter were used to filter the DNS flow-field. For the lowest usual value of  $k_c$  in LES ( $k_c = 8$ ) (Figs. 9a and 9b) discrepancies between the fluctuating acoustic pressure  $p'$ ,  $\tilde{p}'$ , and  $p'^{\text{LES}}$  are observed, where considering both the amplitude and the phase of the signal. This result indicates that the use of the filtered variables to compute the acoustic source term cannot be used for  $k_c \leq 8$  because the unresolved acoustic source term remains significant.

This unresolved noise contribution is reduced when larger values of  $k_c$  are considered (see Figs. 9c and 9d). Nevertheless, the discrepancies between  $\tilde{p}'$  and  $p'^{\text{LES}}$  are still large, indicating that the effect of the SGS must be taken into account.

In all cases, the discrepancies between the fluctuating acoustic pressures  $p'$ ,  $\tilde{p}'$ , and  $p'^{\text{LES}}$  are more significant using the Gaussian filter than the spectral cutoff filter. This can be explained by the nonlocal character of the Gaussian filter in the Fourier space, which allows large eddies to contribute to the SGS, resulting in an increase of the contribution of the SGS to the noise generation process.

The intensity ratio  $I_{\text{SGS}}/\tilde{I} = (\tilde{I} - I_{\text{LES}})/\tilde{I}$  (where  $I_{\text{SGS}}$  and  $I_{\text{LES}}$  are deduced from  $T_{ij}^{\text{SGS}}$  and  $T_{ij}^{\text{LES}}$ , respectively) is reported as a function of  $k_c$  for the two selected filters in Fig. 10 at the two different times considered earlier. The SGS contribution to the resolved acoustic intensity is seen to be important, that is, at least 10% of the total, for cutoff wave numbers  $k_c \leq 12$  at time  $t^* = 4.74$ . As expected, that contribution is much less significant at  $t^* = 5.33$ , but the error is still concentrated on modes  $k \leq 12$ . As already noticed on the fluctuating acoustic pressure, the Gaussian filter induces a larger contribution of the subgrid modes, due to its nonlocal character.

These results indicate in the present computation that the use of the filtered variables to compute the acoustic radiation will lead to an unreliable prediction if the spectral cutoff wave number number is such as  $k_c \leq 8$ , which corresponds to a ratio  $\Delta/L_0 > 0.6$ . For  $8 < k_c \leq 12$ , the source term  $T_{ij}^{\text{SGS}}$  must be taken into account to recover SGS effects. Finally for value of  $k_c$  greater than 12, that is,  $\Delta/L_0 < 0.4$ , the SGS effect is not important, and the computation of the acoustic source term can be carried out without taking into account other effects.

#### IV. Parameterization of Lighthill's SGS Tensor

In the preceding section it has been demonstrated that the SGS tensor in Lighthill's<sup>11,12</sup> equation must be taken into account to

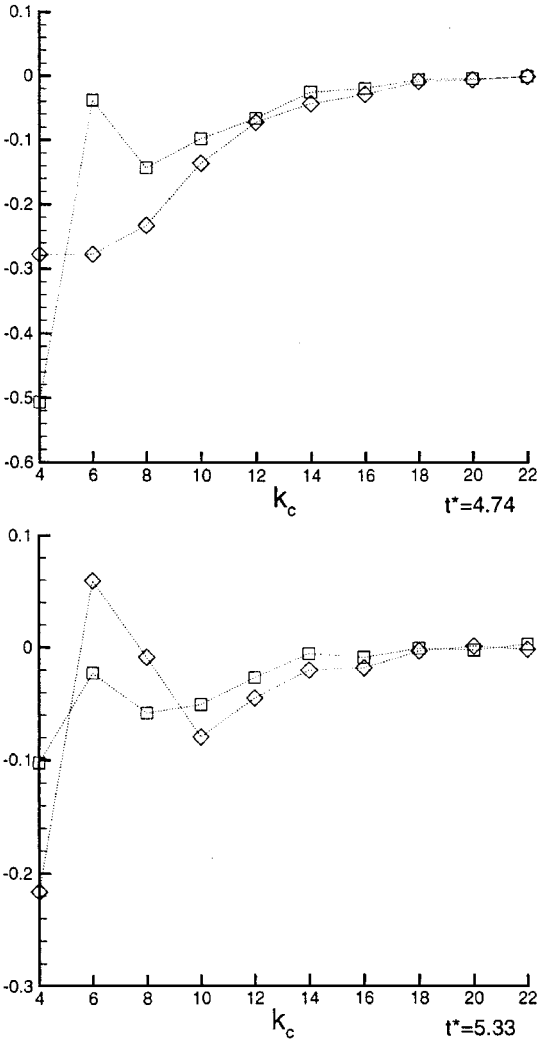


**Fig. 10** Evolution of the SGS intensity  $I^{SGS}/\bar{I}$  as a function of the cutoff wave number  $k_c$  for two different times:  $\square$ , sharp cutoff filter, and  $\diamond$ , Gaussian filter.

recover reliable results. Many ways of modeling the SGS tensor  $\tau_{ij}$  have already been developed.<sup>22,23</sup> Because the Lighthill SGS tensor  $T_{ij}^{SGS}$  has the same expression, the usefulness of these SGS models to correct acoustic variables calculated from  $T_{ij}^{LES}$  is now investigated. If SGS models were perfect, the acoustic field associated with  $\tilde{T}_{ij}$  could be recovered from the LES computation. The exact and approximate SGS fluctuating acoustic pressures ( $p'^{SGS}$  and  $\mathcal{P}'^{SGS}$ ), respectively, computed as a function of  $T_{ij}^{SGS}$  and  $m_{ij}$  (where  $m_{ij}$  is the SGS model for  $T_{ij}^{SGS}$ ) are as follows:

$$p'^{SGS}(x, t) = \frac{1}{4\pi c_0^2} \frac{x_i x_j}{x^3} \int_V \left[ \frac{\partial^2}{\partial t^2} T_{ij}^{SGS} \right] - \left\langle \left[ \frac{\partial^2}{\partial t^2} T_{ij}^{SGS} \right] \right\rangle d^3 y \quad (28)$$

$$\mathcal{P}'^{SGS}(x, t) = \frac{1}{4\pi c_0^2} \frac{x_i x_j}{x^3} \int_V \left[ \frac{\partial^2}{\partial t^2} m_{ij} \right] - \left\langle \left[ \frac{\partial^2}{\partial t^2} m_{ij} \right] \right\rangle d^3 y \quad (29)$$

The corrected fluctuating acoustic pressure is then given by  $\mathcal{P}'(x, t) = p'^{LES}(x, t) + \mathcal{P}'^{SGS}(x, t)$  and must be compared to  $\tilde{p}'(x, t)$ . The resulting acoustic intensity is evaluated as  $I_{LES} + \mathcal{I}_{SGS} = \langle \mathcal{P}'^2(x, t) \rangle / (\rho_0 c_0)$ , where  $\mathcal{I}_{SGS}$  is related to the parameterized SGS tensor (whereas  $I_{SGS}$  is computed using the exact SGS tensor). To estimate the intensity correction given by the SGS model, the ratio  $[\tilde{I} - (I_{LES} + \mathcal{I}_{SGS})]/\tilde{I}$  is compared to  $I_{SGS}/\tilde{I}$ . The ratio can also be written as  $(I_{SGS} - \mathcal{I}_{SGS})/\tilde{I}$  and is identically zero when the exact SGS intensity is recovered. The eddy-viscosity model, scale

similarity model, or a combination of both models is often used to parameterize the SGS tensor occurring in the Navier–Stokes equations. SGS models using an eddy viscosity are based on the hypothesis that the deviatoric part of the  $\tau_{ij}$  is locally aligned with the filtered deviatoric part of the strain tensor, whereas the normal stresses are assumed to be isotropic and are, thus, represented through an SGS kinetic energy. Such models ensure a drain of the kinetic energy but do not reconstitute the characteristic elements (eigenvalues, eigenvector) of the SGS tensor. Indeed, the scale similarity models allow recovery of the characteristic elements (eigenvalues, eigenvector) of the SGS tensor. These models do not dissipate the kinetic energy and are used with eddy-viscosity models together in CFD applications. However, their properties offer an interesting issue for aeroacoustics applications and have been used for the present work.

SGS models of the scale similarity type are based on the hypothesis that the interactions between grid-scale and the SGS modes occur especially between the smallest grid-scale modes and the largest SGS ones and that SGS stresses can be evaluated through an extrapolation in frequency.

The scale similarity model of Refs. 24 and 25 has been used to compute Lighthill's SGS tensor. The corresponding model for the SGS tensor is written as

$$m_{ij} = \bar{\rho}(\tilde{u}_i \tilde{u}_j - \tilde{u}_i \tilde{u}_j) \quad (30)$$

The parameterization of the SGS tensor has been performed only with the Gaussian filter. The model indeed leads to zero when it

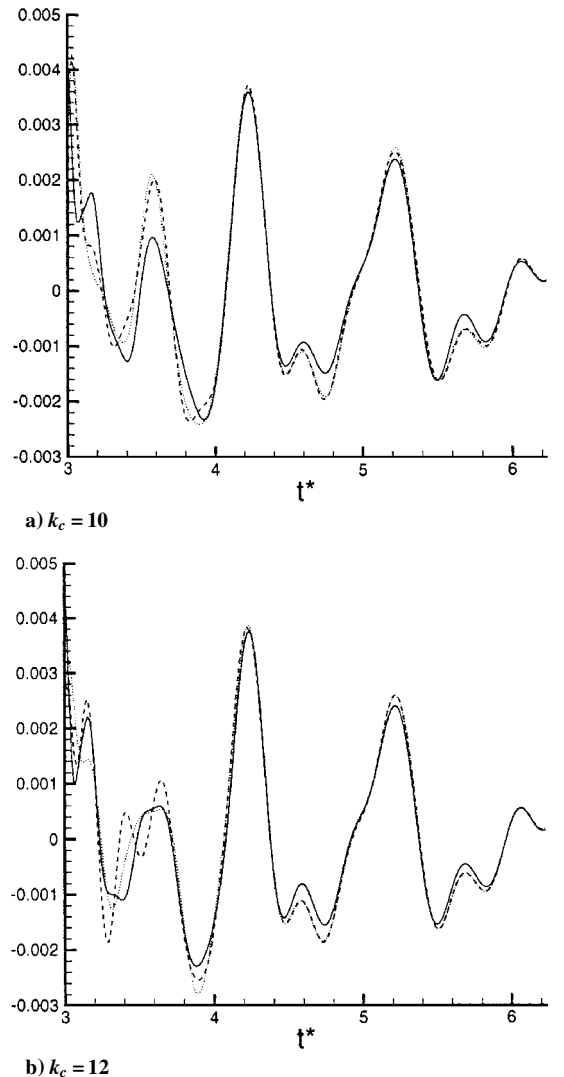


**Fig. 11** Comparison between the fluctuating acoustic pressures  $\text{—}$ ,  $\tilde{p}'$ ;  $\text{- - -}$ ,  $p'^{LES}$ ; and  $\text{...}$ ,  $p'^{LES} + \mathcal{P}'^{SGS}$ , where  $\mathcal{P}'^{SGS}$  has been computed from the Bardina et al.<sup>24,25</sup> model for the Gaussian filter.

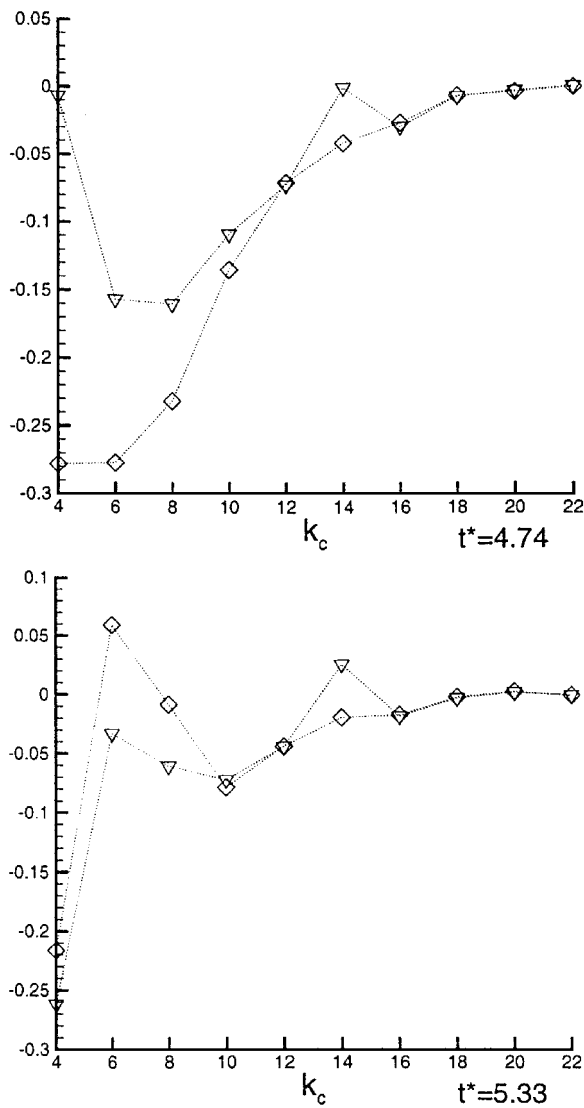


Fig. 12 Comparison the SGS intensity  $I_{SGS}/\bar{I}$  ( $\diamond$ ) and the  $(I_{SGS} - \mathcal{I}_{SGS})/\bar{I}$  ( $\nabla$ ), where  $\mathcal{I}_{SGS}$  has been computed from the Bardina et al.<sup>24,25</sup> model with a Gaussian filter, as a function of cutoff wave number  $k_c$ .

is used together with a sharp cutoff filter. Results dealing with the fluctuating acoustic pressure (Figs. 11a and 11b) show that the model does not induce spurious acoustic pressure fluctuations and provides significant improvements when discrepancies between  $\tilde{p}'$  and  $p'^{LES}$  are important, for example, for  $t^* \approx 3.55$  (Fig. 11b). At this time the rapid oscillation occurring in the fluctuating acoustic pressure is smoothed such that the corrected pressure tends to  $\tilde{p}'$ . The evolution of the intensity ratio  $(I_{SGS} - \mathcal{I}_{SGS})/\bar{I}$  as a function of  $k_c$  is shown in Fig. 12. The correction of the acoustic intensity ratio obtained using the model of Bardina et al.<sup>24,25</sup> is also relevant, the error is reduced to 0–10% for all of the considered values of the cutoff wave number  $k_c$ . Scale similarity models seem to offer a pertinent way to recover the SGS effect for aeroacoustics applications. The results obtained with the Bardina et al. model show that the model contribution depends on the cutoff wave number values; there is an important correction for the small cutoff wave number values, although there is no contribution when all scales are resolved, that is, the large cutoff wave number values. This important conclusion should be relevant for simulations on stretched grid.

## V. Conclusions

To bring out the successive steps to obtain the subgrid acoustic term for hybrid LES calculations, a DNS of decaying isotropic turbulence has been carried out. A new Lighthill equation has been derived from filtered Navier–Stokes equations. The acoustic source term  $(\partial^2/\partial t^2)T_{ij}$  used for DNS computation has been split into three

parts according to Eq. (22): a term  $(\partial^2/\partial t^2)T_{ij}''$  associated to the high-frequency part of the acoustic source that is not resolved in LES calculations, the expected source term for LES based on the filtered basic variables  $(\partial^2/\partial t^2)T_{ij}^{LES}$  and an SGS source term  $(\partial^2/\partial t^2)T_{ij}^{SGS}$ .

To justify that LES calculations can be used to evaluate acoustic sources, the noise generated by the high-frequency part of the source has been estimated and compared to the full noise. Acoustic intensity of the unresolved noise has been computed as a function of the cutoff wave number  $k_c$ . For usual cutoff wave numbers used in LES, the noise generated by the unresolved acoustic source has been found to be negligible.

It has been shown that SGS intensity and the subgrid fluctuating acoustic pressure cannot be neglected for cutoff wave numbers used in LES in the present configuration.

Because the SGS tensor in Lighthill's equation has the same expression as the SGS tensor used for fluid computation  $\tau_{ij}$ , an existing model has been tested. A scale similarity model, the Bardina et al. model, has been chosen for the calculations and has led to reliable results for all cutoff wave number values considered.

## References

- Tam, C. K. W., "Computational Aeroacoustics: Issues and Methods," *AIAA Journal*, Vol. 33, No. 10, 1995, pp. 1788–1796.
- Ribner, H. S., "Quadrupole Correlations Governing the Pattern of Jet Noise," *Journal of Fluid Mechanics*, Vol. 38, No. 1, 1969, pp. 1–24.
- Goldstein, M. E., and Rosenbaum, B., "Effects of Anisotropic Turbulence on Aerodynamic Noise," *Journal of the Acoustical Society of America*, Vol. 54, 1973, pp. 630–645.
- Béchara, W., Lafon, P., Bailly, C., and Candel, S., "Application of a  $k$ - $\epsilon$  Model to the Prediction of Noise for Simple and Coaxial Free Jets," *Journal of the Acoustical Society of America*, Vol. 97, No. 6, 1995, pp. 3518–3531.
- Mitchell, B. E., Lele, S. K., and Moin, P., "Direct Computation of Mach Wave Radiation in an Axisymmetric Supersonic Jet," *AIAA Journal*, Vol. 35, No. 10, 1997, pp. 1574–1580.
- Bastin, F., Lafon, P., and Candel, S., "Computation of Jet Mixing Noise Due to Coherent Structures: The Plane Jet Case," *Journal of Fluid Mechanics*, Vol. 335, 1997, pp. 261–304.
- Bailly, C., Candel, S., and Lafon, P., "Prediction of Supersonic Jet Noise from a Statistical Acoustic Model and a Compressible Turbulence Closure," *Journal of Sound and Vibration*, Vol. 194, No. 2, 1996, pp. 219–242.
- Bailly, C., Lafon, P., and Candel, S., "Subsonic and Supersonic Jet Noise Prediction from Statistical Source Models," *AIAA Journal*, Vol. 35, No. 11, 1997, pp. 1688–1696.
- Witkowska, A., Juvé, D., and Brasseur, J. G., "Numerical Study of Noise from Isotropic Turbulence," *Journal of Computational Acoustics*, Vol. 5, No. 3, 1997, pp. 317–336.
- Manoha, E., Troff, B., and Sagaut, P., "Trailing-Edge Noise Prediction Using Large-Eddy Simulation and Acoustic Analogy," *AIAA Paper 98-1066*, 1998.
- Lighthill, M. J., "On Sound Generated Aerodynamically. Part I: General Theory," *Proceedings of the Royal Society of London*, Vol. A211, 1952, pp. 564–587.
- Lighthill, M. J., "On Sound Generated Aerodynamically. Part II: Turbulence as a Source of Sound," *Proceedings of the Royal Society of London*, Vol. A222, 1954, pp. 1–32.
- Lilley, G. M., "The Generation and Radiation of Supersonic Jet Noise. Vol. IV—Theory of Turbulence Generated Jet Noise, Noise Radiation from Upstream Sources and Combustion Noise. Part II: Generation of Sound in a Mixing Region," U.S. Air Force Aero Propulsion Lab., AFAPL-TR-72-53, July 1972.
- Piomelli, U., Streett, G. L., and Sarkar, S., "On the Computation of Sound by Large-Eddy Simulations," *Journal of Engineering Mathematics*, Vol. 32, 1997, pp. 217–236.
- Sarkar, S., and Hussaini, M. Y., "Computation of the Sound Generated by Isotropic Turbulence," *Inst. for Computer Applications in Science and Engineering*, Rept. 93-74, 1993.
- Favre, A., "Equations Statistiques Aux Fluctuations Turbulentes Dans Les Écoulements Compressibles: Cas Des Vitesses Et Des Températures," *Compte Rendu Académie Sciences de Paris*, Rept. 273, Paris, 1971.
- Vreman, A. W., Geurts, B. J., Kuerten, J. G., and Zandbergen, P. J., "A Finite Volume Approach to Large Eddy Simulation of Compressible, Homogeneous, Isotropic, Decaying Turbulence," *International Journal for Numerical Methods in Fluids*, Vol. 15, 1992, pp. 799–816.
- Brandsma, F. J., "Mathematical and Physics Aspects of Simulation Based on Navier–Stokes Equations," National Aerospace Lab./NLR, ISNAS 88.08.024/NLRTP 89969 L, Amsterdam, 1989.

<sup>19</sup>Sarkar, S., Erlebacher, G., Hussaini, M. Y., and Kreiss, H. O., "The Analysis and Modelling of Dilatation Terms in Compressible Turbulence" *Journal of Fluid Mechanics*, Vol. 227, 1991, pp. 473-493.

<sup>20</sup>Lesieur, M., *Turbulence in Fluids*, 2nd ed., Kluwer Academic, Norwell, MA, 1990.

<sup>21</sup>Moin, P., and Mahesh, K., "Direct Numerical Simulation: A Tool in Turbulence Research," *Annual Review of Fluid Mechanics*, Vol. 30, 1998, pp. 539-578.

<sup>22</sup>Lesieur, M., and Métais, O., "New Trends in Large-Eddy Simulations of Turbulence," *Annual Review of Fluid Mechanics*, Vol. 28, 1996, pp. 45-82.

<sup>23</sup>Rogallo, R. S., and Moin, P., "Numerical Simulation of Turbulent

Flows," *Annual Review of Fluid Mechanics*, Vol. 16, 1984, pp. 99-137.

<sup>24</sup>Bardina, J., Ferziger, J. H., and Reynolds, W. C., "Improved Subgrid Scale Models for Large Eddy Simulation," AIAA Paper 80-1357, 1980.

<sup>25</sup>Bardina, J., Ferziger, J. H., and Reynolds, W. C., "Improved Turbulence Models Based on Large Eddy Simulation of Homogeneous, Incompressible, Turbulent Flows," Thermosciences Div., Dept. of Mechanical Engineering, Rept. TF-19, Stanford Univ., Stanford, CA, 1983.

P. J. Morris  
*Associate Editor*